Ab initio diffuse-interface model for lithiated electrode interface evolution

Maria E. Stournara, Ravi Kumar, Yue Qi, and Brian W. Sheldon

Phys. Rev. E **94**, 012802 — Published 11 July 2016

DOI: 10.1103/PhysRevE.94.012802

Ab initio-based diffuse interface model for lithitated electrode interfaces evolution

Maria E. Stournara[1†*], Ravi Kumar[1†*], Yue Qi[2], Brian W. Sheldon[1]

[1] *School of Engineering, Brown University, Providence, RI 02912, USA*

[2]*Department of Chemical Engineering and Materials Science, Michigan State University, East Lansing, MI 48824 , USA*

Key words: Phase-field modeling, *ab initio* modeling, gradient energy parameter κ, diffuse interface, segregation thickness λ

† Corresponding authors: stournara@fhi-berlin.mpg.de, ravi_kumar@brown.edu

* Equally contributing authors

Abstract

The study of chemical segregation at interfaces, and in particular the ability to predict the thickness of segregated layers via analytical expressions or computational modeling, is a fundamentally challenging topic in the design of novel heterostructured materials. This issue is particularly relevant for the phase-field methodology, which has become a prominent tool for describing phase transitions. These models rely on phenomenological parameters that pertain to the interfacial energy and thickness, quantities that cannot be experimentally measured. Instead of back-calculating these parameters from experimental data, here we combine a set of analytical expressions based on the Cahn-Hilliard approach with *ab initio* calculations to compute the gradient energy parameter κ and the thickness λ of the segregated Li layer at the Si/Cu interface. With this bottom-up approach we calculate the thickness λ of the Li diffuse interface to be on the order of a few nm, in agreement with prior experimental secondary ion mass spectrometry (SIMS) observations. Our analysis indicates that Li segregation is primarily driven by solution thermodynamics, while the strain contribution in this system is relatively small. This combined scheme provides an essential first step in the systematic evaluation of the thermodynamic parameters of the phase-field methodology, and we believe that it can serve as a framework for the development of quantitative interface models in the field of Li-ion batteries.

I. Introduction

Chemical segregation effects at interfaces are among the most intriguing problems in materials science. To control the diffuse interface profiles, computational simulations able to provide an accurate continuum thermodynamic description, such as high throughput *ab initio* simulations, have recently started to gain significant attention. These methods are very effective in describing atomic bonding on discrete interfaces, however diffuse interfaces between two bulk phases present a more substantial computational challenge, largely because they are defined by composition gradients over longer length scales (several nm or more). In these cases, the entire interfacial region cannot be described in a single a*b initio* calculation. To address this limitation, here we develop a hybrid scheme that applies density functional theory (DFT) methods to smaller regions over which the concentration is not constant. These results are then used to obtain a value for the so-called "gradient energy parameter" in the continuum Cahn-Hilliard formulation. We have applied this approach to evaluate recent experimental results which show substantial Li segregation at the interface between lithiated Si and a Cu current collector. More generally, the approach that we present here is important for the development of the phase-field (PF) methodology, which has achieved significant progress [1-9] in the simulation of morphological evolution not only in traditional materials science problems (alloy solidification [10]**,** surface growth [11-13], crystal nucleation [14]), but also in prominent electrochemical problems especially in the field of Li-ion batteries [15-17].

The power of PF methodology essentially pertains to its ability to predict the evolution of arbitrary morphologies and complex microstructures without explicitly tracking the positions of interfaces, while using fundamental information from thermodynamics and kinetics as input [18-21]. The introduction of interface currents and the specific choice of the PF parameters by Karma et al. removed the artifacts due to the diffuse character of the interface and ensured that the convergence of the diffuse interface results in the sharp interface solution [22-24]. Therefore, it rendered PF models a powerful computational approach for modeling on experimentally relevant length and time scales. With this approach the temporal and spatial evolution of the field variables at interfaces are described by linear or non-linear kinetics via the well-known Cahn-Hilliard [21, 25], where the free energy (*F)* of the system is represented by a set of phase field variables, typically the concentrations (*c)* as a function of space and time and their gradients (∇c). The latter represent the diffuse character of the interface, and are included in the model via phenomenological parameters that correspond to the interfacial energy and thickness.

Although in most applications of the PF methodology a realistic description of the interfacial free energy and thickness in terms of spatial dependence is *not* desired for reasons of numerical efficiency,

there are still situations where simulating phase-transition dynamics at small spatial scales (but time scales longer than the ones achieved in molecular dynamics) may be desirable. Such is the case when we wish to predict the *actual* thickness of the interface solely from atomistic calculations (usually on the order of nm or more, i.e. beyond the predictive capability of *ab initio*), which is in line with earlier work some of us did in Ref. [26]. To achieve this, it is necessary to go beyond the common approach of obtaining the gradient energy coefficient κ, by fitting the interfacial energy and the interface width [15, 17] and to proceed with the actual calculation of the parameter. Because the physical origin of the gradient energy term is associated with changes in atomic bonding between neighboring locations and therefore depends on direction, it appears natural that it can be derived from atomistic simulations, even though it is not possible to be directly measured from experimental techniques [1, 15, 17, 27]. Elder et al. where actually the first to combine atomistic simulations with the traditional PF approach in their phase-field crystal (PFC) approach [28, 29] to treat elastic and plastic effects over long timescales. Even in their approach though, the construction of the local free energy density as the order parameter [30] in cases of weak first-order transitions (e.g. solidification from quenched liquids, amorphization of Si due to lithiation), remains a major challenge [31, 32].

This study presents an alternative approach based on combined density functional theory (DFT) and analytical expressions from the Cahn-Hilliard formalism to evaluate the thermodynamic parameters of the Cahn-Hilliard model and from there, derive the diffuse profile interface width, λ. Motivated by our DFT and experimental results in Ref. [26], where we combined modeling and secondary ion mass spectrometry (SIMS) measurements to show that Li segregates on the Si/Cu electrode interface during lithiation, here we extend our analysis to an *ab initio* phase-field model. A complete expression of the Gibbs free energy is derived, where both the effect of the strain built on the Li-segregated layer and the role of the chemical environment are assessed from *ab initio* calculations of dilute and hyper-saturated Li-Si configurations for a certain range of Li concentrations. We show that the mixing enthalpy of the Li-Si compounds is predominantly driven by the chemical reactions in the solution's environment, while the strain contribution in this system is relatively small. Our combined analytical expressions and *ab initio* scheme results in a systematic evaluation of the κ parameter. The predicted thickness λ of the segregated Li rich layer is in very good agreement with prior experimental observations, while the predicted κ parameter based on the *ab initio* scheme also agrees with the back-calculated estimates from the empirical data.

II. Methodology

To evaluate the gradient energy coefficient κ, a continuous Gibbs free energy expression of the Li-Si alloys at *any* Li molar fraction (*x*) is necessary. Though various experimental and modeling attempts for $x \leq 3.75$ have been reported in the literature [33-38], to our knowledge studies on mixing beyond the solubility limit of Li in Si have only been reported for crystalline structures [39, 40]. Here for the first time we model amorphous hyper-saturated phases of Li-Si for $3.75 < x \leq \infty$ via constant volume and temperature (NVT) *ab initio* molecular dynamics (AIMD) calculations with a Nosé thermostat at 1200 K [41, 42] for Li and Si to mix into amorphous phases at various lithium concentrations. We performed AIMD calculations at finite temperature within the framework of density functional theory (DFT), as implemented in the Vienna *ab initio* simulation package (VASP) [43-45]. To represent the change from pure Si to pure Li in this and the following sections, we define concentration *y* for a-Li_xSi, via the expression $y = x/(1+x)$. Therefore, all the compounds can be explored by letting *y* vary between $0 \leq y < 1$. The first four amorphous phases up to $x = 3.75$ ($y = 0.79$) lie below the solubility limit of Li in Si and were generated as indicated in previous work of ours [26] (for further calculation details see Ref. [46-49]) with the corresponding formation energies in agreement with experiments and previous modeling work reported by Chevrier et al. [37]. For statistical accuracy, each amorphous configuration at concentrations below the solubility limit was reproduced three times via AIMD, each time starting from a different configuration. For the hyper-saturated concentrations, the corresponding number of configurations evaluated at each concentration increased to five. Upon the end of each AIMD calculation both the total energy fluctuation and the energy difference between the three equivalent structures was minimal (< 0.25 eV). For each amorphous Li_xSi alloy configuration we chose the lowest energy structure within the AIMD simulation time and relaxed it quantum-mechanically via DFT at 0 K. The lowest energy configuration obtained from DFT represents the hyper-saturated bulk amorphous lithiated Si structure.

III. Results and Discussion

3.1 Formation energy of amorphous Li-Si mixtures above the solubility limit

We have evaluated the contribution of the chemical environment in the Gibbs free energy of a system as

$$\Delta G^{chemical} = \Delta H + PV - T\Delta S_f \quad (1)$$

Since the term PV is in the order of 10^{-5} eV [50, 51], whereas the term $T\Delta S$ is in the order of the thermal energy (26 meV at room temperature), the entropy and pressure terms can be neglected and the free energy will be approximately equal to the enthalpy ΔH of each Li-Si configuration, a value that can be directly evaluated from DFT calculations. Based on the chemical potential model developed by Bucci et al. [52], we derive the contribution of strain in the Gibbs free energy over all states of charge

$$\Delta G^{strain} = (1-y)\int_0^y \left[\frac{-1}{(1-y)^2} \left\{ \frac{\sigma^2}{\rho_{Si}} \frac{\partial\left(\frac{1}{\mathrm{M}}\right)}{\partial\left(\frac{y}{1-y}\right)} + \frac{2\sigma\beta(1-y)}{3(1-y(1-\beta))\rho_{Si}} \right\} \right] dy \qquad (2)$$

where $y = x/(1+x)$; σ is the Cauchy stress in the film $\sigma_{yy} = \sigma_{zz} = \sigma(x)$; M is the biaxial modulus,; and $\beta = V_m^{Li}/V_m^{Si}$. Equation (2) was evaluated with the experimental stress values in Ref. [26] and an expression for the biaxial modulus M as a function of the Li concentration (for details of derivation and the calculation of the biaxial modulus M see App. A).

The free energy profile of various Li-Si binary alloys for $0 \le y < 1$ from DFT calculations is shown in Fig. 1a, along with the energy profile due to strain. Two distinct regions, below and above the solubility limit, are observed. In the first region, where the positive open circuit potential is $\Delta\phi_o$, the composition variation due to the stress component $\Delta y_\sigma = y(\sigma) - y_o$ is minute, compared to the chemical contribution because the mixing of Li and Si is mainly driven by the local chemical environment. That is, the key component responsible for the formation of these compounds is the exothermic character of the lithiation reactions. Indeed, as the system approaches saturation, the dependence on strain reaches $\Delta G_{\max}^{strain} =$ 0.02 eV, while the chemical dependence is greater by almost two orders of magnitude, $\Delta G_{\max}^{chemical} =$ 1.14 eV, indicating that solution thermodynamics have a critical impact on the mixing energy. As some of us showed in previous work on stress contributions in solutions thermodynamics, stress has only a modest impact on the expected Li content of the unsaturated electrode [53]. On the contrary, the magnitude of this effect is primarily limited by the relatively large enthalpy of mixing of Li

and Si, which is also the case here. In the second region, where the solubility limit of Li in Si is surpassed, a miscibility gap between $y_1 = 0.79$ and $y_2 = 0.99$ is formed as shown in Fig. 1a, suggesting that the system phase separates in two thermodynamically stable phases, namely y_1 and y_2. The existence of this depletion region was further corroborated by experimental evidence from SIMS measurements of a CR-2032 coin cell with Si thin film anode (50nm, on Cu current collector) and Li-metal cathode (see experimental details in Ref. [26]). As shown in Fig. B1 in App. B, at deep discharge levels the saturated $Li_{3.75}Si$ phase is immiscible with Li. This is attributed to the excessive amount of Li, which softens the system via the formation of Li-Li bonds [54] without inducing extra stress to the hyper-saturated system. On the contrary, the segregated Li layer at the interface between Si and Cu relaxes the buildup stresses, reducing the contribution of $\Delta G_{\max}^{strain}$ to almost zero values.

3.2 Evaluating the energy gradient coefficient κ and the thickness λ of the Li segregated layer

3.2.1 Theoretical scheme based on *ab initio* data

As demonstrated by Cahn and Hilliard [17], for the solid interface between the Cu surface and lithiated Si, the free energy per unit area is described as the sum of the energy contributions from the *sharp interface* $\Phi(y_s)$ and the *diffuse interface* $\Gamma(y)$

$$\Delta F(y) = \Phi(y_s) + \Gamma(y) = \Phi(y_s) + \int_0^{\infty} \left(\Delta f(y) + \kappa (dy/dz)^2 \right) dz \quad (3)$$

where y_s is the limiting composition $\lim_{y \to 1}$ at the interface ($z = 0$). The second term is the sum of two contributions, one being the free energy referred to as the standard state of *the equilibrium mixture* of Li and Si in a homogeneous solution and the other as *the gradient energy*. Hence, $\Delta f(y)$ is the energy needed to create a unit volume of a uniform solution of composition y from a large reservoir at composition $y_o = y(\infty) = 0.79$ and $\kappa (dy/dz)^2$ is the contribution due to the presence of a concentration gradient. We express the free energy $\Delta f(y)$ for a one dimensional composition change across the interface as the difference between the actual free energy of the Li-Si systems (value in the spinodal region) and that which it would have if the properties of the phases were continuous throughout (common tangent), that is

$$\Delta f(y) = f(y) - f(y_o) - (y - y_o) \left(\frac{\partial f}{\partial y} \right)_{y_o} = \frac{1}{4\kappa} \left(\frac{d\Phi}{dy} \right)^2 \quad (4)$$

Using a dense B-spline fitting to our DFT calculated data (Fig.1), we obtain a continuous function for $\Delta f(y)$. Then, a third order polynomial is fitted to the *ab initio* Li-segregated amorphous Si/Cu interface energies from Ref. [26] to obtain the term $\left(\frac{d\Phi}{dy}\right)$ (details on both fittings in App. C).

We evaluate the dependence of the energy penalty due to gradient energy coefficient κ on the energy density $\Delta f(y)$ and assess the thickness λ of the segregated Li layer at the Li_xSi/Cu interface [26] from

$$\lambda = -\int_{y_s}^{y} \sqrt{\frac{\kappa}{\Delta f(y)}}\, dy \quad (5)$$

with $y_s > y \geq y_o$. For several possible different κ values at $y = y_o$ the results are plotted in Fig. 2a. According to the second term of Eqn. (4), when material is constantly supplied to the interface, the more diffused the interface is, the smaller is the contribution of the gradient energy term $\kappa(dy/dz)^2$. Here we evaluate the dependence of λ on κ *independently* of (dy/dz), as shown in Fig. 2b. The power law relation between the segregated thickness layer and the energy penalty coefficient in Fig. 2c shows that the coefficient κ has a decisive role in the calculation of the segregation thickness λ. This is an essential first step in the evaluation of the λ to κ dependence performed purely from computational calculations. The relation holds certainly for back-calculated κ values from experimental measurements, however here the expression is assessed without inferring any empirical data.

To procced with the calculation of the *actual* value of the κ parameter in the Li-segregated amorphous Si/Cu interface study from Ref. [26], we devised a scheme that applies DFT methods to a small diffused interface regions around a fixed concentration y_o, over which the concentration is not a constant. Note here that although *ab initio* methods are very effective at describing atomic bonding at discrete interfaces, diffuse interfaces between two bulk phases present a substantial computational challenge, largely because they are defined by composition gradients over longer length scales (several nm or more). In these cases, the entire interfacial region cannot be described by a single *ab initio* calculation, therefore one needs to proceed with calculations in smaller regions with a concentration gradient. To simulate this diffused interface at the atomic level, we modelled the concertation gradient near the spinodal region at $y_o = 0.9$ via substitution of Si (Li) with Li (Si) atoms on the left (right) side of a bisected unit cell of cross section $A = 1\ \text{nm}^2$, as shown in the schematic in Fig. 1(b-d). Relaxing the

atoms in the cell and minimizing the energy locally will in fact "freeze" each relaxed structure into a concentration gradient, instead of reaching a uniform concentration (which will only occur if long time AIMD is performed). This way, the energy of each structure was calculated as a deviation from the uniform behavior and the slope (dy/dz) was obtained from fitting to the results obtained from a binning analysis along the z-direction. The bin widths range from 2.75 to 2.85 Å and are comparable to the first nearest neighbor bonding distance Li-Li (2.5−2.9 Å), Li-Si (2.75−2.9 Å), and Si-Si (2.75−2.9 Å) in the bulk a-Li_xSi configurations. Note that the criteria for the selection of y_o are on one hand that y_o is around the concentration of interest (in our case in the spinodal region) and on the other hand that we can efficiently simulate the gradient (dy/dz) with DFT, i.e. there needs to be a sufficient amount of Si atoms in the model structure to simulate the gradient, hence very rich Li configurations are not a wise choice. Here, we show results for a model of N_{tot} = 160 atoms, but the same trend holds for a larger model of 240 atoms as shown in App. D.

The physical origin of the gradient energy term is associated with changes in atomic bonding from one location to neighboring ones. As the gradient term appears naturally in a limit transition to the continuum of the discrete counterparts of the gradient thermodynamics, it can be derived from DFT results, where the linear increase in energy holds independently of the number of atoms used in the model. To calculate the gradient energy coefficient κ, we integrate the diffuse interface term $\Gamma(y)$ from Eqn. (3) over the length z of the unit cell, i.e.

$$\Gamma(y) = \int_0^z \left(\Delta f(y) + \kappa (dy/dz)^2\right) dz \quad (5)$$

As shown in Table I, for the Li-segregated amorphous Si/Cu interface study of interest we obtain $\kappa \approx 10^{-7}$ J m^{-1}. Eventually, from Eqn. (4) we calculate that the thickenss of the segregated Li layer at the interface of Cu and lithiated Si is 7.24 nm. To assess our theoretical scheme we also back-calculate λ from empirical data based on prior experimental observations, as shown in the following section.

3.2.2 Experimental evaluation of the segregated Li layer

To experimentally evaluate λ we employed SIMS measurements on a lithiated Si/Cu interface [26]. The density of Li in Li_xSi, ρ_{Li} can be written as

$$\rho_{Li} = \frac{n_m}{V_m} = \frac{x}{V_0 + Kx} \quad (6)$$

with the molar volume of Li_xSi, V_m being

$$V_m = \frac{1}{1+x} V_0 + \frac{x}{1+x} K \quad (7)$$

where V_o is the unlithiated molar volume of Si and K is the molar volume of Li in Si, whose values were taken from Ref. [55]. Integration with the trapezoid rule over the area under the SIMS measured data in Fig. 3a results in the amount of Li buildup at the Si/Cu interface

$$\sum_{i=1}^{n} \frac{1}{2}\left(\rho_{Li_k} + \rho_{Li_{k+1}}\right)\Delta\lambda = \lambda_2 \rho_{Li}^{\ Li_{3.75}Si} + \lambda_1 \rho_{Li}^{\ Li_x Si} \quad (8)$$

To calculate the thickness of segregation we used a bilayer approximation (Fig. 3b), where the layer closer to the interface is Li-rich (thickness λ_1) and the adjacent layer is at $y_o = 0.79$ (x=3.75, thickness λ_2) so that

$$\lambda = \lambda_1 + \lambda_2 \quad (9)$$

Then λ can be obtained from solving the system of Eqns. (8) and (9). Due to the diffuse nature of the Li-segregated layer it is not easy to define the position of the interface between the lithiated Si and the Cu substrate. To address this issue, we consider two scenarios based on Fig. 3a: One where the interface lies where the Cu signal starts increasing and one where it lies at the crossing of the Li/Si and Cu signals. Note that although the effect of Li-smearing was not taken into account in the bilayer approximation and a sharp interface for the calculation of the segregation layer was considered instead, Fig. 3c shows there is a range of possibilities for the thickness of the segregated layer depending on the molar fraction of Li, y. When $\lim_{y_s \to 1}$, that is when the nature of the segregated layer is considered to be almost pure Li (as it was for the DFT results), the corresponding thickness is in the order of 4.2-7.5 nm depending on the interface position, indicating excellent agreement with the computationally calculated thickness.

In previous DFT calculations we showed that due to partial electron transfer from Li to the Cu surface, a short-range attractive interaction is built between the negatively charged Cu surface and the positively charged Li ions, inducing segregation of Li at the Li_xSi/Cu interface [26]. This results in the formation of a metastable Li-Si mixture at some high Li concentration in the hyper-saturated region, which can be thought of as a smeared interface due to the existence of long-range interactions. Note that as DFT methods can only capture short-range interactions, the evaluation of long-range interactions remained elusive until the current model, which combines efficiently atomistic and higher order interactions in a complete description. This study demonstrates that a scheme based on analytical phase field model expressions that use *ab initio* inputs directly, can be employed for the prediction of the thickness of the Li diffuse interface provided that the limiting concentration y_s is properly considered in

the model. In Table II, we summarize the findings obtained from the *ab initio* calculation, the analytical solution based on the DFT Gibbs free energy expression and the experimental measurements.

IV. Summary

In summary, we present a systematic approach based on *ab initio* calculations and analytical expressions, which provides accurate predictions of the two key parameters in Cahn-Hilliard diffuse interface models, namely the gradient energy coefficient κ and the thickness λ of the diffuse interface. Our scheme was evaluated for hyper-saturated Li-Si configurations in a wide range of Li concentrations. We calculated the thickness of the Li segregated layer from Ref. [26] in agreement with prior experimental SIMS observations, where these quantities are back-calculated from empirical data. To achieve this, we derived a complete expression of the Gibbs free energy and predicted that the mixing enthalpy of the Li-Si compounds is predominantly driven by the chemical reactions in the solution's environment, i.e. the formation of Li-rich networks and the breaking of Li-Si and Si-Si bonds can lead to strongly exothermic and endothermic reactions far more critical to the mixing, compared to the strain contributions. Our formalism provides an accurate description of the nature of the lithiated Si/Cu interface based on phase-field principles, and can serve as a framework for the development of theoretical quantitative interface models.

Acknowledgements

We gratefully acknowledge the support from National Science Foundation under Grant No. DMR-1410850 and 1410946 for the collaborative research.

Appendices

Appendix A: Derivation of the strain component, ΔG^{strain}

For any property B (e.g. U, S, V, H, F and G) in a binary system with y being the molar fraction ranging from $0 \leq y \leq 1$ as defined earlier, we can write

$$\Delta\overline{B_1} = \Delta B_{mix} + (1 - y_1)\frac{d\Delta B_{mix}}{dy_1} \quad (A1)$$

Considering $\overline{B_1} = \overline{G_{Li}} = \mu_{Li}$ we can derive the following expression

$$\mu_{Li} - \mu_{Li}^{o} = \Delta G_{mix} + (1 - y)\frac{d\Delta G_{mix}}{dy} \quad (A2)$$

Bucci et al. performed numerical simulations to characterize the mechanical and electrochemical response of thin film amorphous Si electrodes during cyclic lithiation [52] and suggested that the chemical potential of Li in Si (in Li_xSi) can be expressed as

$$\mu_{Li} - \mu_{Li}^{o} = RTln\frac{\gamma x}{x_{max} - x} - \frac{\sigma^2}{\rho_{Si}}\frac{\partial\left(\frac{1}{M}\right)}{\partial x} - \frac{2\sigma\beta}{3(1+\beta x)\rho_{Si}} \quad (A3)$$

Where, $= n_{Li}/n_{Si} = y/(1-y)$, x_{max} is the concentration ratio in the fully lithiated state, M is biaxial modulus, σ is stress in the film, $\beta = molar\ volume\ of\ Li/molar\ volume\ of\ Si = 0.82$, $\rho_{Si} = 7.874\ X10^4 moles \cdot m^{-3}$

By simplifying the ODE, we get

$$\frac{d(\frac{\Delta G_{mix}}{1-y})}{dy_{Li}} = \frac{1}{(1-y)^2}\left\{RTln\frac{\gamma y(1-y_{max})}{y_{max}-y} - \frac{\sigma^2}{\rho_{Si}}\frac{\partial\left(\frac{1}{M}\right)}{\partial(\frac{y}{1-y})} - \frac{2\sigma\beta(1-y)}{3(1-y(1-\beta))\rho_{Si}}\right\} \quad (A4)$$

Simple consideration of the effect of stress on ΔG_{mix}, simplifies the equation into

$$\frac{d\left(\frac{\Delta G^{strain}}{1-y}\right)}{dy_{Li}} = \frac{-1}{(1-y)^2}\left\{\frac{\sigma^2}{\rho_{Si}}\frac{\partial\left(\frac{1}{M}\right)}{\partial(\frac{y}{1-y})} + \frac{2\sigma\beta(1-y)}{3(1-y(1-\beta))\rho_{Si}}\right\} \quad (A5)$$

Integration of Eqn. (A5) results in

$$\Delta G^{strain} = (1-y)\int_0^y\left[\frac{-1}{(1-y)^2}\left\{\frac{\sigma^2}{\rho_{Si}}\frac{\partial\left(\frac{1}{M}\right)}{\partial(\frac{y}{1-y})} + \frac{2\sigma\beta(1-y)}{3(1-y(1-\beta))\rho_{Si}}\right\}\right]dy \quad (A6)$$

To solve Eqn. (A6) the following two values are necessary:

1. The stress (σ) as a function of concentration of Li
2. The biaxial modulus (M) as a function of concentration of Li

As the stress state in Si thin film is of elastic-plastic nature, deriving an analytical form of the stress as a function of Li concentration is a non-trivial task. However, from the experimental measurements reported in the recent work by Stournara et al. for Li molar fraction as high as y = 0.79 [26], extrapolation to y = 1.0 is possible by fitting a curve to the experimentally observed stress with respect to Li concentration. For simplicity, the stress was considered to be of the following form:

$$\sigma = 1.99y - 2.00 \quad GPa \qquad (A7)$$

The biaxial modulus was obtained from a linear approximation fit to the experimental data published in Ref. [56], as shown in Fig. A1. From linear fitting the experimental data we get

$$\frac{1}{M} = -3.69 \text{ X } 10^{-3} \frac{y}{1-y} + 1.66 \text{ X } 10^{-2} \quad (A8)$$

By substituting σ and 1/M from Eqns. A7 and A8 into equation A6, we were able to solve the integral equation and the result; change in free energy as a function of Li concentration due to stress, is plotted in Fig. 3 of the paper, along with the chemical effect.

Appendix B: Experimental evidence of Li segregation

The coin cell was cycled at a rate of C/100 using current of ~0.5 μA and reached open circuit voltage below 0V, as shown in Fig. B1. At 0.05V the system is saturated in Li. From that point on, the excessive amount of Li segregates in the form of a discrete phase, shown by the plateau region at -5mV. The negative voltage is indicative of Li plating, suggesting that at deep discharge levels where the saturated $Li_{3.75}Si$ phase is immiscible with Li, the excessive amount of Li softens the system via the formation of Li-Li bonds [39], without inducing extra stress to the hyper-saturated system. On the contrary, the segregated Li layer at the interface between Si and Cu relaxes the buildup stresses, reducing the contribution of $\Delta G_{\max}^{strain}$ to almost zero values.

Appendix C: Continuous functions fitting on DFT calculations

Here we calculate the composition profile and the excess free energy due to the interface by finding the function $y(z)$ which minimizes the excess free energy of a unit area of interface from the expression

$$\Delta f(y) = f(y) - f(y_o) - (y - y_o)\left(\frac{\partial f}{\partial y}\right)_{y_o} = \frac{1}{4\kappa}\left(\frac{d\Phi}{dy}\right)^2 \quad \text{(C1)}$$

We start by evaluating the left-hand term, i.e. $f(y) - f(y_o) - (y - y_o)\left(\frac{\partial f}{\partial y}\right)_{y_o}$. The function $f(y)$ is then evaluated from spline fitting to the calculated *ab initio* energy values in 22 y_{Li} regions for 0.78 ≤ y ≤ 1.0. The fitted curves in each region are a third order polynomial, i.e. $f(y) = Ay^3 + By^2 + Cy + D$, that maintains continuity at the boundaries of the different regions till the second derivative as shown in Fig. C1. To evaluate the right-hand term, we express the variation of the interfacial energy, Φ at the Li_xSi/Cu interface with Li concentration. To solve equation C1, we obtain the term $\left(\frac{d\Phi}{dy}\right)$ by fitting the *ab initio* data with a 3rd degree polynomial (Fig. C2). With both $f(y)$ and $\left(\frac{d\Phi}{dy}\right)$ evaluated, the surface concentration y_s which minimizes the excess free energy was calculated for a range of κ parameters and its dependence on their values was evaluated.

Appendix D: *Ab initio* results for structures with a concentration gradient

As shown in Fig. D1, the linear increase in energy holds independently of the number of atoms used in the model, showing that the concentration gradient that induces this deviation from the homogeneous state, is responsible for the formation of less energetically favorable configurations.

References

1. Moelans, N., B. Blanpain, and P. Wollants, *An introduction to phase-field modeling of microstructure evolution.* Calphad-Computer Coupling of Phase Diagrams and Thermochemistry, 2008. **32**(2): p. 268-294.
2. Li, Y.L., et al., *Phase-field model of domain structures in ferroelectric thin films.* Applied Physics Letters, 2001. **78**(24): p. 3878-3880.
3. Tang, M., W.C. Carter, and R.M. Cannon, *Diffuse interface model for structural transitions of grain boundaries.* Physical Review B, 2006. **73**(2).
4. Kassner, K., et al., *Phase-field modeling of stress-induced instabilities.* Physical Review E, 2001. **63**(3).
5. Bhate, D.N., A.F. Bower, and A. Kumar, *A phase field model for failure in interconnect lines due to coupled diffusion mechanisms.* Journal of the Mechanics and Physics of Solids, 2002. **50**(10): p. 2057-2083.
6. Chen, L.Q. and W. Yang, *COMPUTER-SIMULATION OF THE DOMAIN DYNAMICS OF A QUENCHED SYSTEM WITH A LARGE NUMBER OF NONCONSERVED ORDER PARAMETERS - THE GRAIN-GROWTH KINETICS.* Physical Review B, 1994. **50**(21): p. 15752-15756.
7. Elder, K.R., et al., *Sharp interface limits of phase-field models.* Physical Review E, 2001. **64**(2).
8. Guyer, J.E., et al., *Phase field modeling of electrochemistry. I. Equilibrium.* Physical Review E, 2004. **69**(2).
9. Guyer, J.E., et al., *Phase field modeling of electrochemistry. II. Kinetics.* Physical Review E, 2004. **69**(2).
10. Boettinger, W.J., et al., *Phase-field simulation of solidification.* Annual Review of Materials Research, 2002. **32**: p. 163-194.
11. Elder, K.R., et al., *Modeling elasticity in crystal growth.* Physical Review Letters, 2002. **88**(24).
12. Karma, A. and M. Plapp, *Spiral surface growth without desorption.* Physical Review Letters, 1998. **81**(20): p. 4444-4447.
13. Pierre-Louis, O., *Phase field models for step flow.* Physical Review E, 2003. **68**(2).
14. Granasy, L., T. Borzsonyi, and T. Pusztai, *Nucleation and bulk crystallization in binary phase field theory.* Physical Review Letters, 2002. **88**(20).
15. Cogswell, D.A. and M.Z. Bazant, *Coherency Strain and the Kinetics of Phase Separation in LiFePO4 Nanoparticles.* Acs Nano, 2012. **6**(3): p. 2215-2225.
16. Bai, P., D.A. Cogswell, and M.Z. Bazant, *Suppression of Phase Separation in LiFePO4 Nanoparticles During Battery Discharge.* Nano Letters, 2011. **11**(11): p. 4890-4896.
17. Han, B.C., et al., *Electrochemical modeling of intercalation processes with phase field models.* Electrochimica Acta, 2004. **49**(26): p. 4691-4699.
18. Allen, S.M. and J.W. Cahn, *MICROSCOPIC THEORY FOR ANTIPHASE BOUNDARY MOTION AND ITS APPLICATION TO ANTIPHASE DOMAIN COARSENING.* Acta Metallurgica, 1979. **27**(6): p. 1085-1095.
19. Fischer, F.D., J. Svoboda, and H. Petryk, *Thermodynamic extremal principles for irreversible processes in materials science.* Acta Materialia, 2014. **67**: p. 1-20.
20. Penrose, O. and P.C. Fife, *THERMODYNAMICALLY CONSISTENT MODELS OF PHASE-FIELD TYPE FOR THE KINETICS OF PHASE-TRANSITIONS.* Physica D, 1990. **43**(1): p. 44-62.
21. Cahn, J.W. and J.E. Hilliard, *FREE ENERGY OF A NONUNIFORM SYSTEM .3. NUCLEATION IN A 2-COMPONENT INCOMPRESSIBLE FLUID.* Journal of Chemical Physics, 1959. **31**(3): p. 688-699.
22. Karma, A. and W.J. Rappel, *Phase-field method for computationally efficient modeling of solidification with arbitrary interface kinetics.* Physical Review E, 1996. **53**(4): p. R3017-R3020.

23. Karma, A. and W.J. Rappel, *Quantitative phase-field modeling of dendritic growth in two and three dimensions.* Physical Review E, 1998. **57**(4): p. 4323-4349.
24. Karma, A., *Phase-field formulation for quantitative modeling of alloy solidification.* Physical Review Letters, 2001. **87**(11).
25. Liang, L., et al., *Nonlinear phase-field model for electrode-electrolyte interface evolution.* Physical Review E, 2012. **86**(5).
26. Stournara, M.E., et al., *Li segregation induces structure and strength changes at the amorphous Si/Cu interface.* Nano Letters, 2013. **13**(10): p. 4759–4768.
27. Niu, J., et al., *In Situ Observation of Random Solid Solution Zone in LiFePO4 Electrode.* Nano Letters, 2014. **14**(7): p. 4005-4010.
28. Elder, K.R. and M. Grant, *Modeling elastic and plastic deformations in nonequilibrium processing using phase field crystals.* Physical Review E, 2004. **70**(5).
29. Elder, K.R., et al., *Phase-field crystal modeling and classical density functional theory of freezing.* Physical Review B, 2007. **75**(6).
30. Asadi, E. and M.A. Zaeem, *A Review of Quantitative Phase-Field Crystal Modeling of Solid-Liquid Structures.* Jom, 2015. **67**(1): p. 186-201.
31. Archer, A.J., et al., *Solidification fronts in supercooled liquids: How rapid fronts can lead to disordered glassy solids.* Physical Review E, 2012. **86**(3).
32. Robbins, M.J., et al., *Modeling the structure of liquids and crystals using one- and two-component modified phase-field crystal models.* Physical Review E, 2012. **85**(6).
33. Kim, H., et al., *Structure and properties of Li− Si alloys: a first-principles study.* The Journal of Physical Chemistry C, 2011. **115**(5): p. 2514-2521.
34. Rohrer, J. and K. Albe, *Insights into degradation of Si anodes from first-principle calculations.* The Journal of Physical Chemistry C, 2013. **117**(37): p. 18796-18803.
35. Chou, C.-Y. and G.S. Hwang, *Surface effects on the structure and lithium behavior in lithiated silicon: A first principles study.* Surface Science, 2013. **612**: p. 16-23.
36. Cubuk, E.D. and E. Kaxiras, *Theory of structural transformation in lithiated amorphous silicon.* Nano letters, 2014. **14**(7): p. 4065-4070.
37. Chevrier, V.L. and J.R. Dahn, *First Principles Model of Amorphous Silicon Lithiation.* Journal of the Electrochemical Society, 2009. **156**(6): p. A454-A458.
38. Zhang, Q., Y. Cui, and E. Wang, *First-principles approaches to simulate lithiation in silicon electrodes.* Modelling and Simulation in Materials Science and Engineering, 2013. **21**(7): p. 074001.
39. Morris, A.J., C.P. Grey, and C.J. Pickard, *Thermodynamically stable lithium silicides and germanides from density functional theory calculations.* Physical Review B, 2014. **90**(5).
40. Tipton, W.W., et al., *Structures, phase stabilities, and electrical potentials of Li-Si battery anode materials.* Physical Review B, 2013. **87**(18).
41. Balke, N., et al., *Real Space Mapping of Li-Ion Transport in Amorphous Si Anodes with Nanometer Resolution.* Nano Letters, 2010. **10**(9): p. 3420-3425.
42. Johari, P., Y. Qi, and V.B. Shenoy, *The Mixing Mechanism during Lithiation of Si Negative Electrode in Li-Ion Batteries: An Ab Initio Molecular Dynamics Study.* Nano Letters, 2011. **11**(12): p. 5494-5500.
43. Kresse, G. and J. Furthmuller, *Efficiency of ab-initio total energy calculations for metals and semiconductors using a plane-wave basis set.* Computational Materials Science, 1996. **6**(1): p. 15-50.
44. Kresse, G. and J. Furthmuller, *Efficient iterative schemes for ab initio total-energy calculations using a plane-wave basis set.* Physical Review B, 1996. **54**(16): p. 11169-11186.

45. Kresse, G. and D. Joubert, *From ultrasoft pseudopotentials to the projector augmented-wave method.* Physical Review B, 1999. **59**(3): p. 1758-1775.
46. Starting from the initial bulk amorphous configurations, the cells were allowed to equilibrate at 1200K for roughly 5000 MD time steps, with an MD step of 3 fs. A time of approximately 15 ps proved to be sufficient for substantial mixing in agreement with results reported in our previous work [26]. For statistical accuracy, each amorphous configuration was reproduced three times via AIMD. Upon the end of each AIMD calculation both the total energy fluctuation and the energy difference between the three equivalent structures was minimal (< 0.5 eV). For each a-Li_xSi configuration we chose the lowest energy structure and further relaxed them quantum-mechanically through DFT at 0 K. The lowest energy configuration obtained from DFT was chosen to represent the hyper-saturated bulk amorphous Li_xSi structure.
47. Perdew, J.P., K. Burke, and M. Ernzerhof, *Generalized gradient approximation made simple.* Physical Review Letters, 1996. **77**(18): p. 3865-3868.
48. Feynman, R.P., *Forces in molecules.* Physical Review, 1939. **56**(4): p. 340-343.
49. We used projector-augmented-wave (PAW) potentials [45] to mimic the ionic cores, and the generalized gradient approximation (GGA) in the Perdew-Burke-Ernzerhof (PBE) flavor [47] for the exchange and correlation functional. The plane-wave energy cutoff is 300.0 eV for all the bulk a-Li_xSi structures and the a-Li_xSi/Cu interfaces based on convergence tests. The convergence tolerance for the electronic relaxation was 10^{-5} eV/ cell and the total energy was calculated with the linear tetrahedron method with Blöchl corrections. All structural relaxations employed conjugate gradient methods to minimize energy of the structure and the required Hellmann– Feynman force [48] on each atom was less than 0.01 eV A^{-1}.
50. Aydinol, M.K. and G. Ceder, *First-principles prediction of insertion potentials in Li-Mn oxides for secondary Li batteries.* Journal of the Electrochemical Society, 1997. **144**(11): p. 3832-3835.
51. Aydinol, M.K., et al., *Ab initio study of lithium intercalation in metal oxides and metal dichalcogenides.* Physical Review B, 1997. **56**(3): p. 1354-1365.
52. Bucci, G., et al., *Measurement and modeling of the mechanical and electrochemical response of amorphous Si thin film electrodes during cyclic lithiation.* Journal of the Mechanics and Physics of Solids, 2014. **62**: p. 276-294.
53. Sheldon, B.W., et al., *Stress Contributions to Solution Thermodynamics in Li-Si Alloys.* Electrochemical and Solid State Letters, 2012. **15**(1): p. A9-A11.
54. Shenoy, V.B., P. Johari, and Y. Qi, *Elastic softening of amorphous and crystalline Li-Si Phases with increasing Li concentration: A first-principles study.* Journal of Power Sources, 2010. **195**(19): p. 6825-6830.
55. Obrovac, M.N., et al., *Alloy design for lithium-ion battery anodes.* Journal of the Electrochemical Society, 2007. **154**(9): p. A849-A855.
56. Sethuraman, V.A., et al., *In situ measurements of stress evolution in silicon thin films during electrochemical lithiation and delithiation.* Journal of Power Sources, 2010. **195**(15): p. 5062-5066.

Table I: The gradient energy coefficient κ parameter for $N_{at}^{tot} =$ 160 and 240 at $y_o = 0.90$

a*b initio* model	**ΔE (eV)**	**A∫Δf.dZ (eV)**	**dy/dz (m^{-1})**	**κ (eV m^{-1})**	**κ (J m^{-1})**
160 atoms, 6 bins	2.24	-1.56	$-4.62 \cdot 10^{7}$	$6.36 \cdot 10^{11}$	$1.02 \cdot 10^{-7}$
240 atoms, 6 bins	3.94	-0.29	$-2.41 \cdot 10^{7}$	$2.61 \cdot 10^{12}$	$4.18 \cdot 10^{-7}$

Table II: Analytical, computational and experimental results for the thickness λ of the segregated Li layer

Method	**Thickness λ (nm)**
- Analytical model (based on ΔG)	6.87
- DFT simulation (based on calculations at y_s=0.9)	7.24
- SIMS measurement	4.2-7.5

Figures

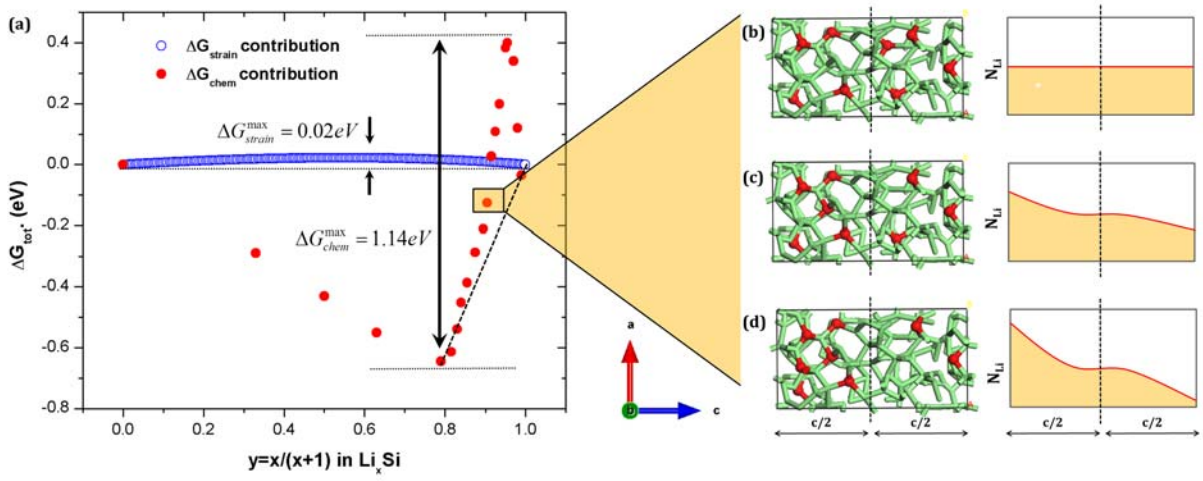

Fig.1: *Ab initio* results for saturated and hyper-saturated systems and the modeled concentration gradient at y = 0.9. **(a)** ΔG as a function of the state of charge y. Contributions from strain are presented in black open circles and those from the chemical environment in red full circles. A blue dashed line bounds the unstable region where spinodal decomposition occurs; **(b-d)** Li-Si configurations at y = 0.9 along with a schematic for the Li concentration gradient across the interface (shown with a dashed line) at c/2 to demonstrate uniform and non-uniform systems. Li: green atoms, Si: red atoms (total number of atoms N_{at} = 160).

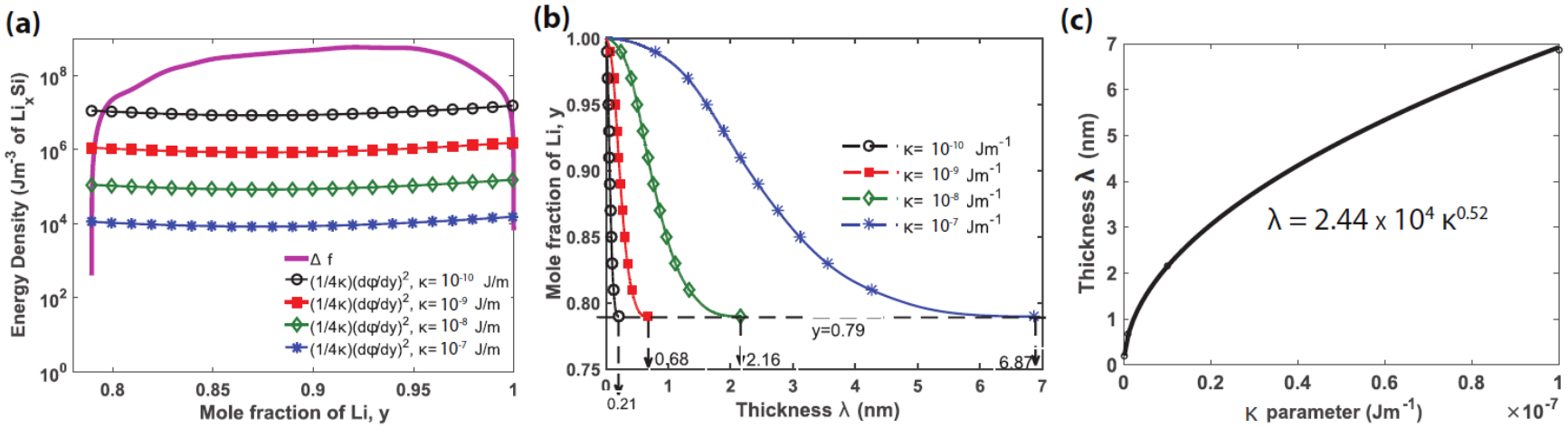

Fig. 2: Analytical evaluation of the thermodynamic parameters κ and λ. **(a)** Energy density as a function of the molar fraction y. The points where the two curves meet represent solutions to Eqn.4 for different values of κ; **(b)** Dependence of the Li mole fraction on the thickness of the segregated layer λ for various κ values; **(c)** Power law dependence of the segregated thickness λ on the thermodynamic parameter κ. Based on this expression and the *ab initio* models at *y=0.9*, the predicted thickness for the Li layer in Ref. [26] is calculate to be in the order of 7.24 nm.

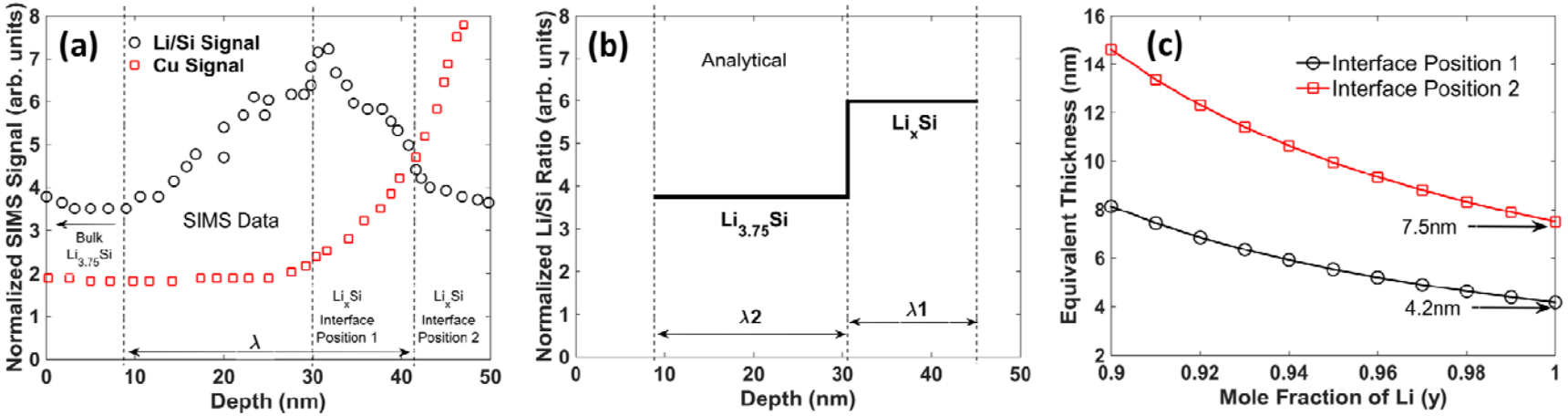

Fig. 3: SIMS measurement and experimental evaluation of the thickness. **(a)** SIMS depth profile of Li/Si ratio through the thickness of a lithiated Si film on Cu from Ref. [26]; **(b)** Schematic of bilayer approximation for the calculation of the thickness λ of the segregated layer ; **(c)** Thickness λ of the segregated layer for two interface positions scenarios.

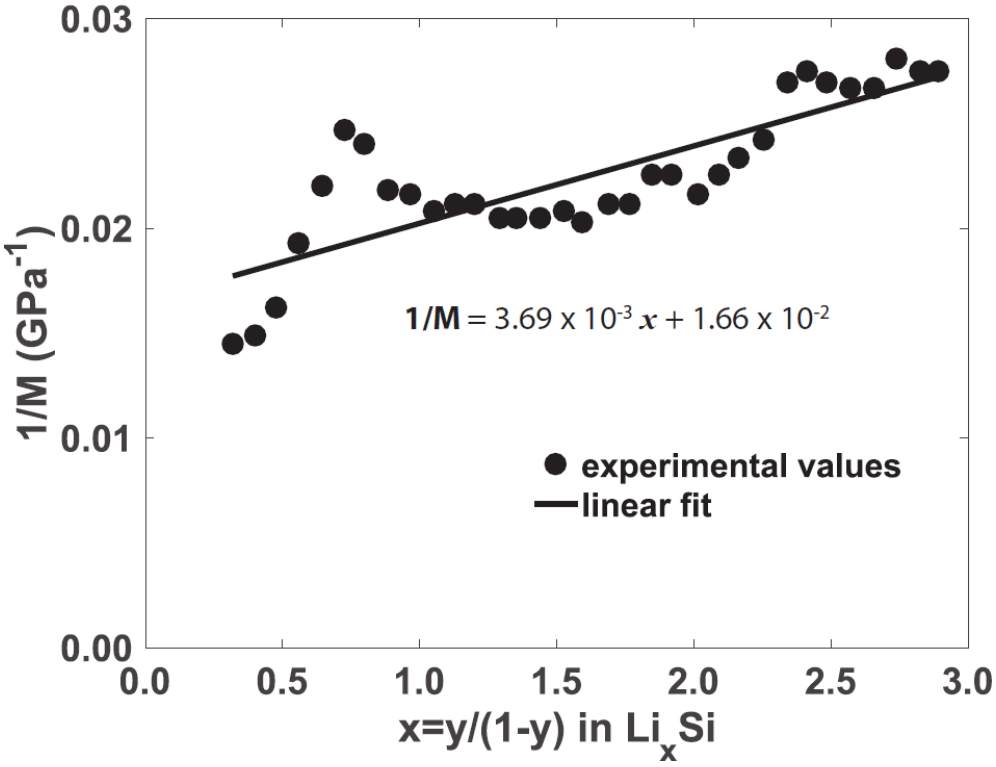

Fig. A1: Experimentally observed biaxial modulus and fitted curve

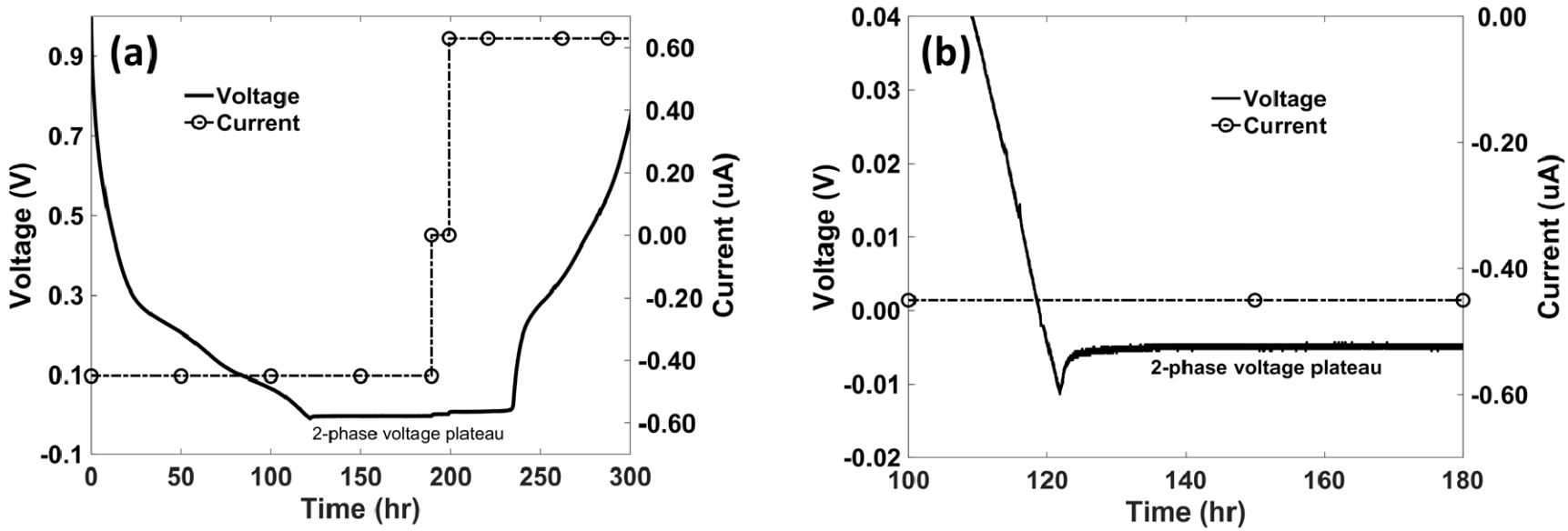

Fig. B1: a) First cycle behavior of 50nm thin film of Si b) expanded view of voltage plateau observed during lithiation in 1st cycle

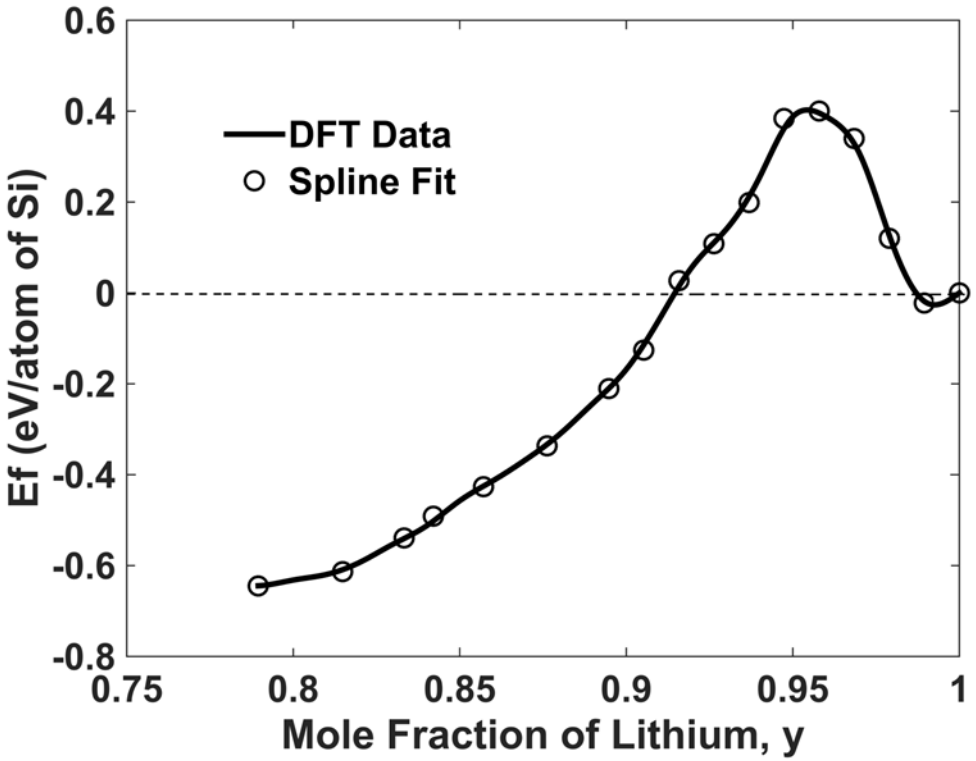

Fig. C1: Formation Energy of Li_xSi showing DFT data points and also spline fit

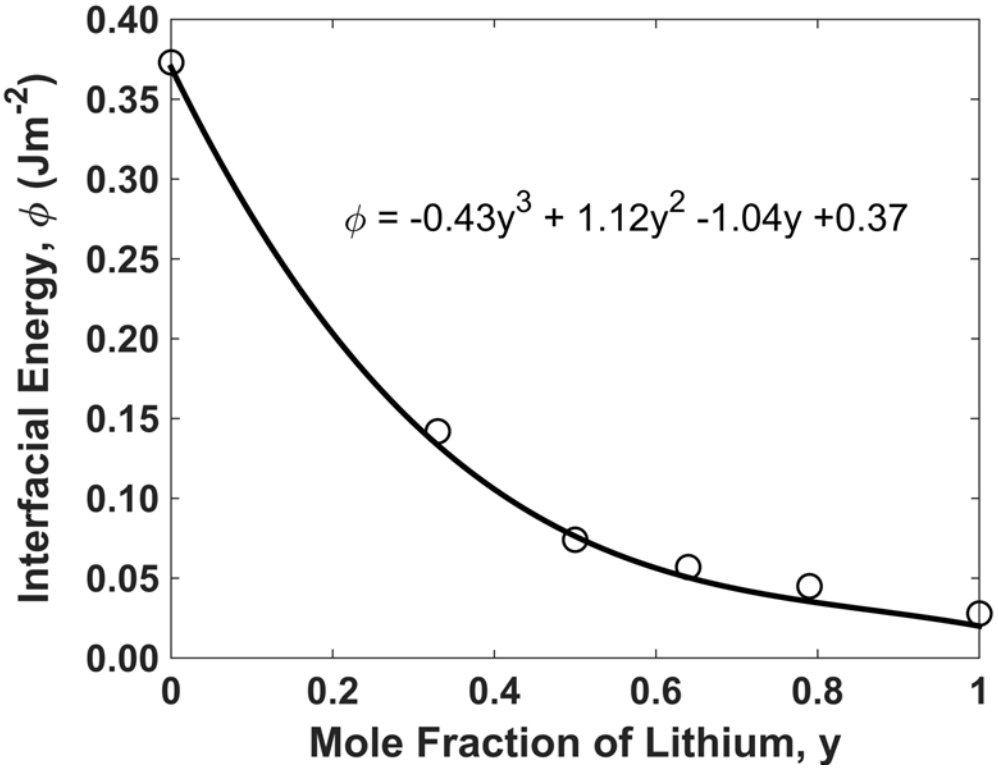

Fig. C2: Variation of interfacial energy Φ of Li_xSi/Cu with Li concentration

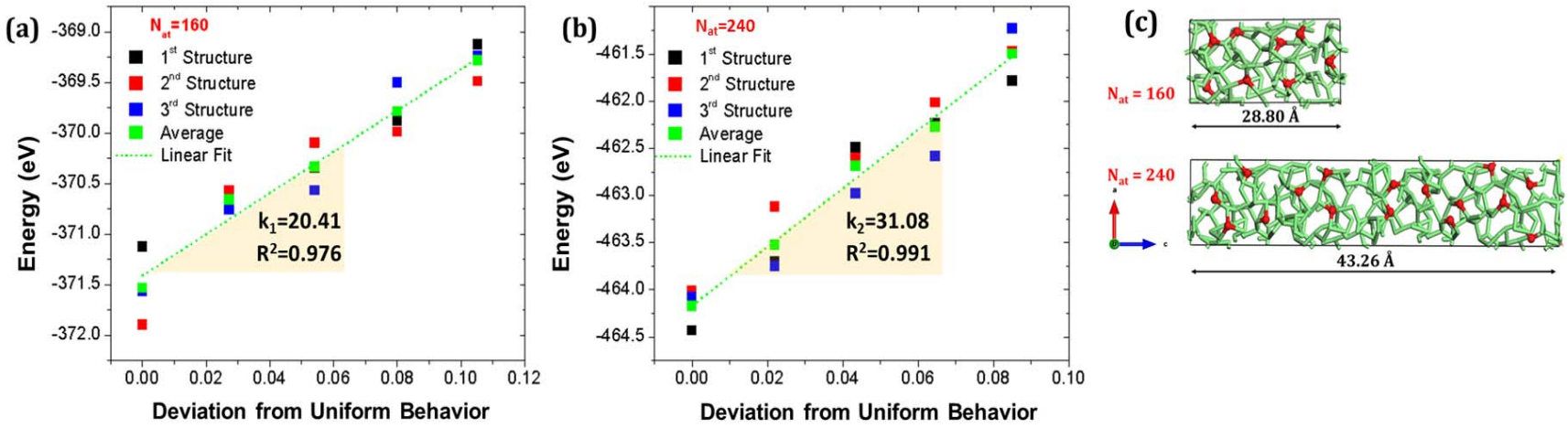

Fig. D1: Li-Si configurations at y = 0.9 with a gradient in the Li concentration across the interface at c/2 (shown with a green dashed line). Li: green atoms, Si: red atoms. Energies reported for (a) N_{at}=160 atoms, and (b) N_{at}=240 atoms. Both models demonstrate similar behavior with the trends maintained. In (c) the full length and cross section of area A of the three 3D-models used. Li: green atoms, Si: red atoms.